IEEE Access
Multidisciplinary | Rapid Review | Open Access Journal

Received August 16, 2021, accepted September 9, 2021, date of publication September 10, 2021,
date of current version September 21, 2021.

Digital Object Identifier 10.1109/ACCESS.2021.3112107

Design, Development, and Characterization of a Low Frequency CMUT-Based Anemometer

MAYANK B. THACKER[1], (Graduate Student Member, IEEE), AREZOO EMADI[2], (Senior Member, IEEE), AND DOUGLAS A. BUCHANAN[1], (Senior Member, IEEE)

[1]Department of Electrical and Computer Engineering, University of Manitoba, Winnipeg, MB R3T 5V6, Canada
[2]Department of Electrical and Computer Engineering, University of Windsor, Windsor, ON N9B 3P4, Canada

Corresponding author: Mayank B. Thacker (thacker5@myumanitoba.ca)

This work was supported by the National Science and Engineering Research Council of Canada (NSERC).

ABSTRACT The design fabrication and development of a 67.5 kHz capacitive micromachined ultrasonic transducer (CMUT) suited for Martian anemometry is presented in this paper. To have low signal attenuation under Martian conditions, the device operating frequency is limited to 100 kHz. This is due to the low-density carbon dioxide (CO_2) atmosphere and acoustic impedance mismatch transduction losses. CMUTs capable of generating frequencies less than 100 kHz need either large Silicon area or higher operating voltages. This is a problem for the battery operation and portability of devices. The devices presented in this paper are designed and fabricated using low cost commercially available surface micromachining technique. COMSOL Multiphysics and MATLAB simulations were used to analyze the device critical design parameters and investigate the operability of devices. Simulation results show that the designed single cell 170-μm radius membrane has a resonant frequency $\sim$65 kHz. The device exhibits a static displacement of 105nm under 20 V DC bias. Using the developed single cell model, a 3×10 array CMUT anemometer was fabricated and evaluated that generates a $\sim$65 kHz acoustic signal in lab environment. This proposed CMUT anemometer can operate for a supply < 38 V. The device performance was evaluated using a commercial air-coupled capacitive microphone named CAP1. Successful transmit-receive of ultrasound from the developed 2D array to CAP1 for separation in the range of 1-15 cm was performed. The experiment results performed in lab environment show the speed of sound and the atmospheric attenuation can be accurately measured using this developed technology with a $\pm 5\%$ accuracy.

INDEX TERMS CMUTs, low frequency, MEMS, PolyMUMPs, polysilicon membrane, ultrasound.

I. INTRODUCTION

An anemometer is used for wind speed measurements. Anemometers are broadly classified into mechanical or electronic. Ultrasonic anemometry is a type of electronic technique which uses ultrasound signal generation and reception [1]. Ultrasound is used in various applications since past century [2]–[4]. Martian anemometry is now focused on this ultrasonic anemometry technique [1]. An ultrasonic anemometry uses time of flight calculations to estimate the wind speed. This is done by placing the transmitting and receiving transducers apart by a fixed distance [5], usually $\sim$12 cm. An increase in the wind speed, increases the ultrasonic wave velocity and vice-versa. Thus, the wind speed is directly relatable to the time taken for a wave to travel the distance between transmitter and receiver. An ultrasound-based anemometry is a type of electronic technique that has contactless operation and avoids the drawbacks of other techniques [5], [6] like the hot wire and hot film [7].

An ultrasound can be generated using piezoelectric devices. Many piezo based ultrasonic transducers are commercially available that can operate in the given frequency range [8], [9]. However, the piezo transducers have a higher acoustic impedances ($\sim$30 Mrayl) leading to poor matching and therefore power loss [10]. Therefore, to use piezo devices, an extra impedance matching layer is needed, increasing the fabrication complexity. A capacitive micromachined ultrasonic transducer (CMUT) is also used for ultrasound generation [11]. CMUTs provide better acoustic

The associate editor coordinating the review of this manuscript and approving it for publication was Sanket Goel.

matching [12]–[14], making them well suited for Martian atmospheric conditions [1], [5].

CMUTs are constructed by having a clamped membrane, over a fixed bottom electrode. The electrical supply is directly connected to these two as shown in Fig. 1. The gap between the two layers is air or vacuum [15]. To generate ultrasound from a CMUT, a DC voltage superimposed by an AC is applied across the membrane and bottom electrode. The applied DC voltage functions as the pull-in voltage [12]. An additionally applied ac signal causes the membrane to vibrate around its resonant frequency [16]. The possible bending of a conventional membrane under the influence of a DC supply is shown is Fig. 1 by dashed lines. Fig. 1 also illustrates the generation of ultrasound signal from a movable membrane.

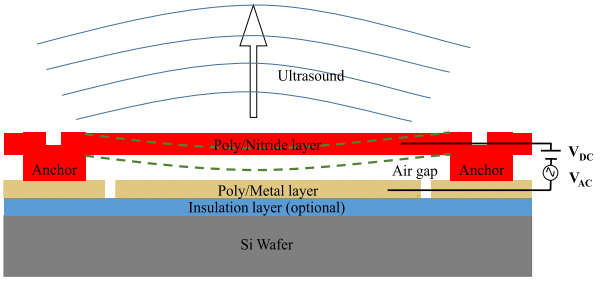

FIGURE 1. CMUT and the generation of ultrasound.

The effective radius of the membrane is inside of anchors, shown as dashed lines in Fig. 1, which can vibrate. The design has an opening in anchor for the electrical connection to the lower membrane. The electrostatic force acting on the top membrane is found using equation 1 [15], [16].

$$F_{electrostatic} = \frac{\varepsilon_0 A V_{DC}^2}{2d^2} + \frac{\varepsilon_0 A V_{DC} v_{ac}}{d^2} \tag{1}$$

where, A is the area of the lower membrane, V_{DC} is the DC bias and v_{ac} is the ac signal voltage, and d is the air gap between the two membranes.

Researchers have developed CMUTs that operate below 100 kHz frequency range [13], [17], [18]. However, the CMUTs described in [13], [17], and [18], either have dimensions larger than 4-mm or have operating voltages more than 170 V. Considering the application to be Martian environment, where portability and operation in stipulated power is a major confinement [1], the existing devices are difficult to use, when connected in arrays. The design and development of such a CMUT that has lower operating voltage, 37 V, and smaller dimension, 170-μm radius, for generation of desired frequency ultrasound, is addressed in this paper.

As the CMUTs presented in this work are envisioned for Martian ultrasound-based anemometry, their frequency of operation is limited to <100 kHz [5]. This is due to the low-density CO_2 atmosphere on Mars has high attenuation as compared to Earth air and the acoustic impedance mismatch transduction losses. The developed devices are designed to operate at a resonant frequency of 67.5 kHz that is below the maximum limit. This frequency also has the least possible signal attenuation in Martian environment [1]. Therefore, these CMUT anemometer can be tested in a simulated Martian environment of ~95% CO_2 and pressure ~600 Pa [19]. The technique presented, is low cost, small size and will help eliminate the sensitivity and response time related issues associated with other anemometry techniques, like hot-film or hot-wire [1], [5], [6].

II. LOW FREQUENCY CMUT DESIGN AND FABRICATION

The CMUT membrane structure proposed in this paper was designed and fabricated using a commercially available MEMSCAP Inc., PolyMUMPs process. This fabrication is a surface micromachining process, which comprises of three structural and two sacrificial layers. The polysilicon structural layers are denoted as Poly0, Poly1 and Poly2 whereas the sacrificial layer as Oxide1 and Oxide2 [20].

The PolyMUMPs provided film parameters that were used for analytical calculations and for COMSOL Multiphysics finite element modelling (FEM) are presented in Table 1. The resonant frequency of the CMUT device, shown in Fig. 1, is calculated using equation 2 [21].

$$f_r = \frac{1}{2\pi}\sqrt{\frac{1}{M}\left(\frac{16\pi E h^3}{3\left(1-\nu^2\right)R^2} - \frac{\varepsilon A {V_{DC}}^2}{d_0^3}\right)} \tag{2}$$

TABLE 1. Film parameters and device dimensions.

Poly1/Top membrane thickness	2 µm
Membrane diameter	340 µm
Density of Polysilicon membrane	2320 kg/m^3
Polysilicon Poisson's ratio	0.22
Polysilicon Young's modulus	158 GPa
Air gap	2 µm
Poly0/Lower contact thickness	0.5 µm

where, f_r is the resonant frequency, h is the membrane thickness, R is the radius, A is the membrane area, M is the mass and d_0 is the air gap between the two membranes. The membrane mass is dependent on the material density. E and ν are the Young's modulus and Poisson's ratio for the membrane material, respectively. The term enclosed in parenthesis, in equation 2, is called as the spring constant. As the applied DC voltage is increased, the structure becomes more elastic and the resonant frequency decreases. As a designer using PolyMUMPs, only the radius and applied voltage were available to vary to achieve the desired resonant frequency of CMUT devices. The other parameters like E, ν, d_0, and h were process dependent or parameters like A, and M were directly related to radius.

The schematic view of the proposed CMUT device designed in MEMSPro is shown in Fig. 2, where the membrane is supported by the annulus shaped anchors.

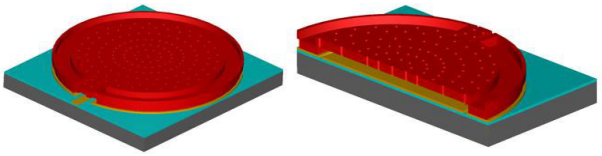

FIGURE 2. 3D model of the device presented in this paper made in MEMSPro. A similar 3D geometry model was constructed in COMSOL for simulations.

This structure uses two polysilicon layers, from the available three layers of the PolyMUMPs process. The PolyMUMPs process was followed to fabricate the devices. Poly1 layer (red color) forms the membrane, the Poly0 layer (golden color) is the fixed bottom electrode. An isolation layer using silicon nitride (blue color) was deposited beneath the Poly0 layer to avoid charge leakage to the silicon substrate. All the layers, including sacrificial, were deposited using low-pressure chemical vapor deposition (LPCVD) [20]. Electrical connections were made directly to the two poly layers. The holes, as seen in top membrane in Figs. 2(a) and 2(b), were formed lithographically in the top structural layer. They served to allow access of the chemical etchant to the sacrificial layer. These etch holes were positioned not more than 30 μm apart and from each other and the support anchor. The chips were dipped in 49% concentrated hydrofluoric acid (HF) solution to etch the sacrificial layers. A deionized (DI) water rinse and alcohol rinse followed the etch. The process concluded with a 10 min, 110°C anneal in oven. A supercritical drying step with CO2 was used to avoid any issues due to device stiction[20] The membrane parameters [20] and dimensions are listed in Table 1. It was a challenge to fabricate and bias membrane devices of such a large diameter and size, as large membranes tend to bend under their own weight, sometimes sufficiently to touch the lower contact.

COMSOL Multiphysics were employed to simulate the device resonant frequency and the membrane displacement under DC conditions. A 3D geometry model, shown in Fig. 2, of the proposed structure was constructed in COMSOL, having two polysilicon layers separated by air gap. The gap and dimensions of the layers are already shown in Table 1. Structural mechanics was used to study the effect of applied voltage and the electrostatic force acting on the top membrane. In the COMSOL simulations, the exterior borders of the top layer were set as fixed constraint. However, the layer itself was free to deform thus was set as an elastic material. An electric potential was applied between the top and the bottom layers. A displacement of 105 nm was observed for 20 V DC as shown in Fig. 3.

The etch holes in the device were neglected during COMSOL simulations, reducing the number of meshing elements, aiding in quicker simulations. However, in another simulation, etch holes were added and there was less than 10% difference in the eigen frequency results with and without the etch holes. This is because the total area occupied by etch holes was $<8\%$ of the membrane area. The first

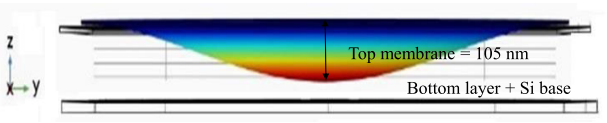

FIGURE 3. Membrane displacement for proposed device in COMSOL for 20V DC.

eigen frequency of the structure was observed at 170 kHz. Using equation 2 and the device dimensions it was found that the device can operate below 100 kHz for bias voltage exceeding 33V. Further increasing this bias to closer to the pull-in voltage 37V, the resonance frequency attainable was ~53 kHz. The collapse voltage of the designed device was found to be 38 V.

An optical image of the fabricated device displaying the etch hole placement is shown in Fig. 4.

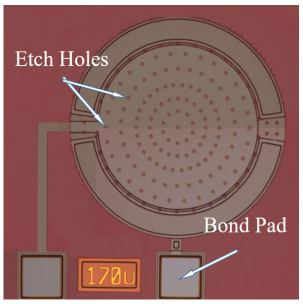

FIGURE 4. Optical image of the fabricated device having 170 μm radius.

The structure shown in Fig. 4, was fabricated as a single cell device, as well as a 1D array of 10 devices and a 2D array of 3×10 on the same chip. A single cell device is insufficient to generate enough acoustic output. Therefore, a 2D array was fabricated by connecting the individual devices. The 2D structure is analogous to an RF antenna where the radiator is at the center and a perfectly absorbing medium present surrounding it. Therefore, antenna principles can be applied to study the performance of the arrays. Using MATLAB simulations, the directivity of the fabricated 2D array was estimated. MATLAB's transducer array calculation (TAC) utility was used, and the parameters were set for 65 kHz sine wave, 343 m/sec as the speed of sound for a 3×10 array of devices covering a 4.1mm^2 area having needed dimensions and separations. The simulation results are shown in Fig. 5.

As seen in Fig. 5, the maximum ultrasound is focused only on the front side of the array. Maximum output is obtained at the front center part of the arrangement at 7 cm from the center. This helped in estimating the near field/ far filed transition point for the fabricated device, discussed under acoustic characterization.

III. ELECTRICAL CHARACTERIZATION

The impedance responses of the CMUT chips were electrically characterized using the Agilent's 4294A precision impedance analyzer. The transducers resonance was observed

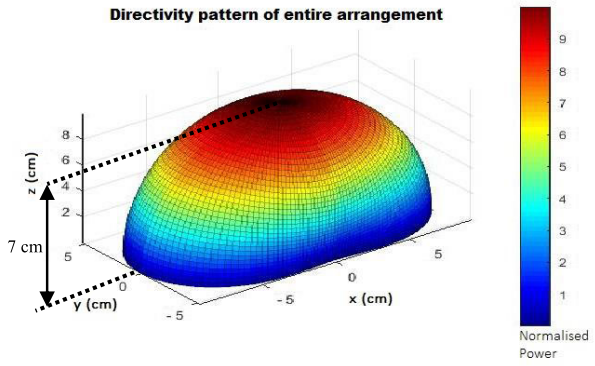

FIGURE 5. Directivity of the 2D arrangement found by TAC utility in MATLAB.

in terms of impedance, which was a function of DC bias for a fixed ac bias. The ac signal, 1 V_{p-p}, was superimposed on the DC bias. The DC bias was varied from 16-37 V. This range was selected as there were very less impedance changes below 16 V and the device collapse voltage was 38 V. The collapse voltage of the device agreed with the COMSOL simulation results. The ac signal frequency was swept from 20 kHz to 300 kHz which was through the 1st eigen frequency of the transducer. For each bias voltage, the real part of the impedance is used to extract the device resonant frequency.

In Fig. 6, the real part of impedance for a single device is shown, whereas in Fig. 7 the similar measurement for a 2D array is displayed. As seen in both Figs. 6 and 7 the DC bias was varied, and the resonant peaks were observed. The increase in DC bias, lowered the resonance frequency of the device [22]. This is due to the spring softening effects and can be found from Eqn. 2. It is observed from Fig. 6 and 7, once the DC bias exceeds 32 V DC, the device resonant frequency falls into the desired frequency range, below 100 kHz. Thus, using a proper bias the device can be set to operate for the desired ∼65 kHz frequency. For the 2D array, the individual devices are connected as a combination of 3 parallel rows of 10 devices in series. Thus, the impedance measurements of the 2D array appears less than that of a single device. The resonant frequency shift as a function of applied DC bias is shown in Fig. 8. The bias frequency peaks were found from the impedance data used to plot Fig. 6 and 7. The frequency shifts are a function of the square of the applied DC bias. The spring softening effect is clearly observed in Fig. 8.

IV. ACOUSTIC CHARACTERIZATION

The 2D CMUT array was tested acoustically to assess their performance. Pitch-catch measurements were carried by using the CMUT array as an ultrasonic wave transmitter and a commercial capacitive transducer (CAP1) from VN Instruments ltd. as the receiver. The CAP1 operates between 30-90 kHz frequency range, which was suitable for testing the device array biased to operate at lower frequency.

For testing, the chip was mounted on a test fixture, which was then mounted on a XYZ positioner. An external

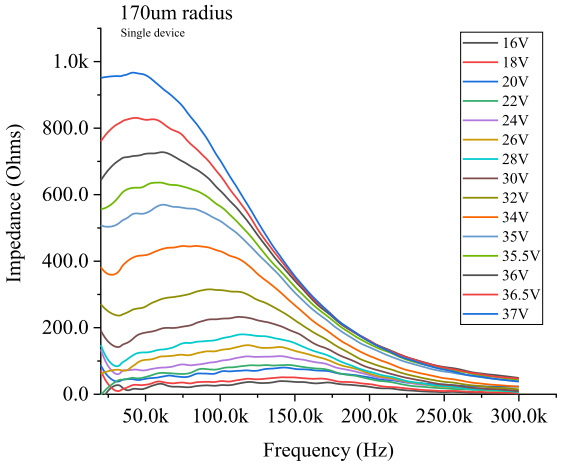

FIGURE 6. Real part of impedance for 170 μm radius single device.

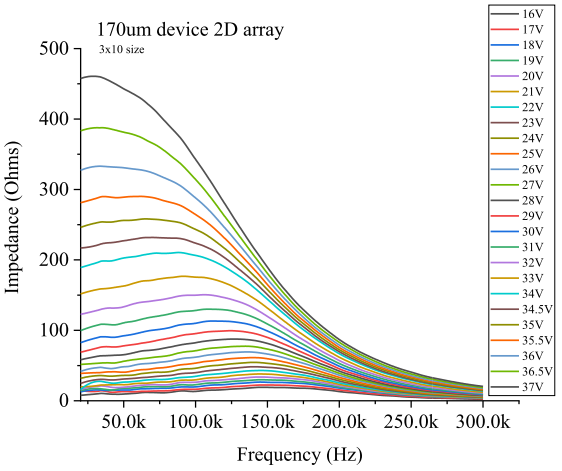

FIGURE 7. Real part of impedance for 2D array with 170 μm radius devices.

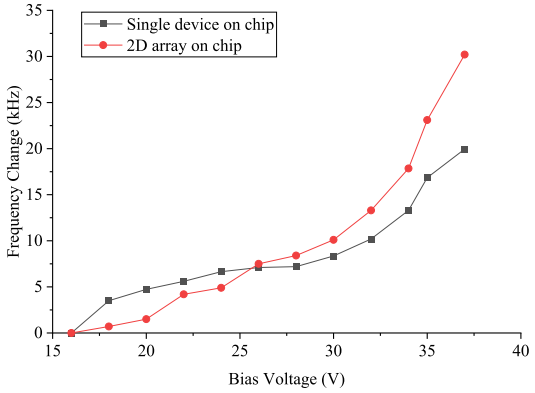

FIGURE 8. Resonant frequency shift with bias.

controller regulated the movements of the XYZ positioner. A holder was used to hold the CAP1 transducer, and an adjustable supporting rod was used for height adjustments. This pitch-catch setup is shown in Fig. 9. A Keithley 237 high voltage source unit was used for the DC supply and an

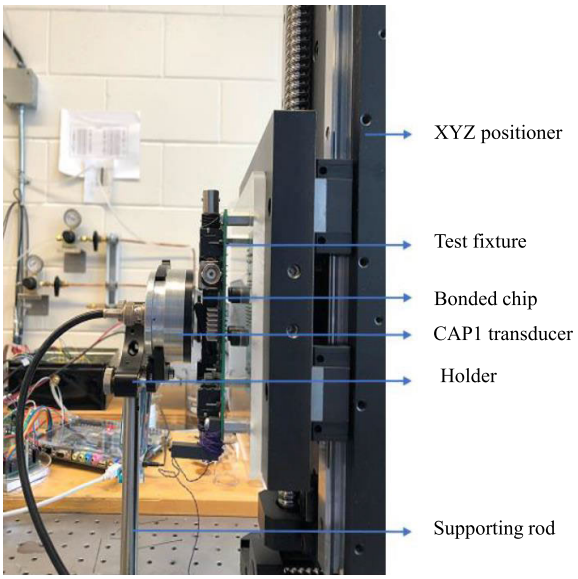

FIGURE 9. Pitch-catch setup.

Agilent 33220A arbitrary waveform generator was used as an ac signal source. The schematic diagram of this apparatus is shown in Fig. 10.

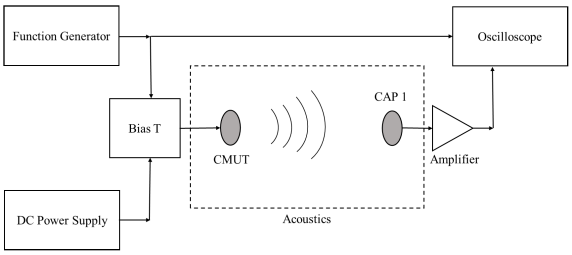

FIGURE 10. Device connections for pitch-catch.

The receiver side had a remote module from VN instruments Ltd. which had a built-in amplifier circuit. The gain of the amplifier was set to 90 dB. An Agilent DSO-X 3014A digital oscilloscope was used to measure and record both the transmitted and received waveforms.

For the acoustic measurements, the DC and ac bias were fixed at 35 V and 2 V_{p-p} signal, respectively. The total voltage supplied was set such that it did not exceed the breakdown voltage of 38 V. At this bias, the device was operating in the needed frequency range and was producing acoustic output that was easily detected. The highest output, for the setup shown in Fig. 10, for a fixed DC supply voltage and transducer separation, was observed at 67.5 kHz. Thus, the ac frequency for acoustic measurements was set to 67.5 kHz. An AC signal burst of 5 cycles was generated using the waveform generator. This combination of AC and DC was fed to the 2D array via a bias-T. In Fig. 11, an example of the transmitted and received signals are illustrated. The transmitter-receiver separation for this experiment was set

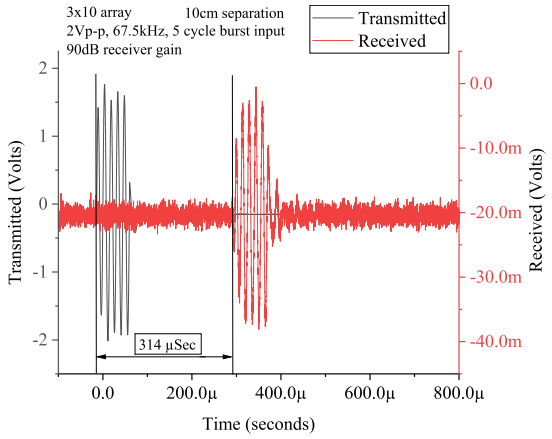

FIGURE 11. Transmitted and received wave for 10 cm separation.

to 10 cm. The measurements were made in lab environment at 20°C.

A series of experiments were performed where this axial separation was varied from 1 cm to 15 cm and the corresponding "time of flight" was measured as the time for the acoustic wave to travel from the transmitter to the receiver. Using the measurement data, sound velocity was found for lab environment from the slope of the signal time versus distance as shown in Fig. 12.

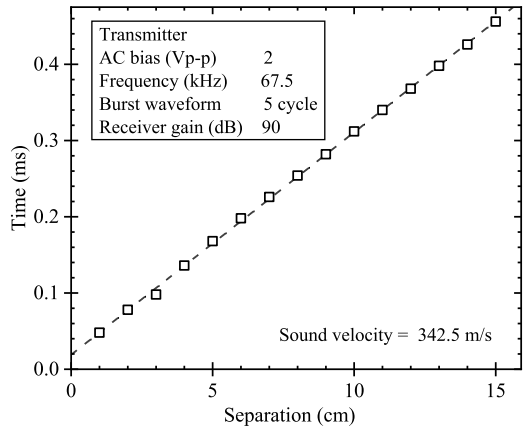

FIGURE 12. Speed of sound estimation.

The amplitude of the received signal was also noted as a function of varying the separation between transmitter and receiver in the range 1-15 cm. This was to assess the signal attenuation in air. Thus, the amplitudes are plotted as a function of the separation and are shown in Fig. 13.

The output voltage, from the amplified received signal, initially increases until a separation of 7 cm, after which the signal decreases. This is due to the near/far field transitions, also seen in the MATLAB simulations for calculating signal directivity discussed earlier, Fig. 5. The limit of the near field can be given by equation 3 shown below [23],

$$N = \frac{D^2 F}{4V} \tag{3}$$

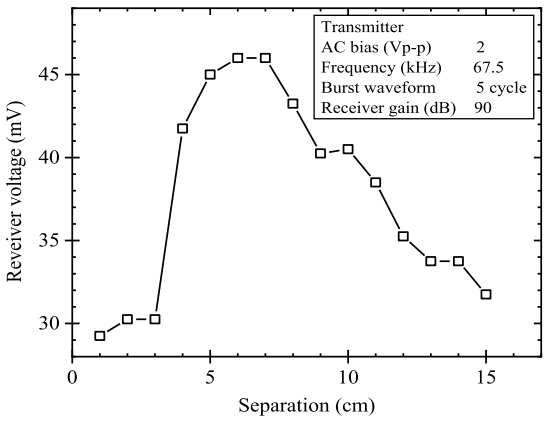

FIGURE 13. Received acoustic signal voltage vs separation.

where, N is the near/far field transition point, D is the diameter of the transducer, F is the frequency of operation and V is the velocity of sound in a given material, air in this case. Substituting the values, the CAP1 has a diameter of 3.8 cm, F as 67.5 kHz, and V as 343 m/sec into equation 3, yield a value of N = 7.3 cm. From the results presented here, the amplitude of the received signal begins to decrease very close to calculated value of 7.3 cm. The atmospheric attenuation is calculated from the slope of the curve as a function of the log of the received signal voltage and separation, resulting from the exponential drop in signal strength. This is plotted in Fig.14, the slope of which is found to have the attenuation. This is used for validating the CMUTs acoustic amicability with the environment.

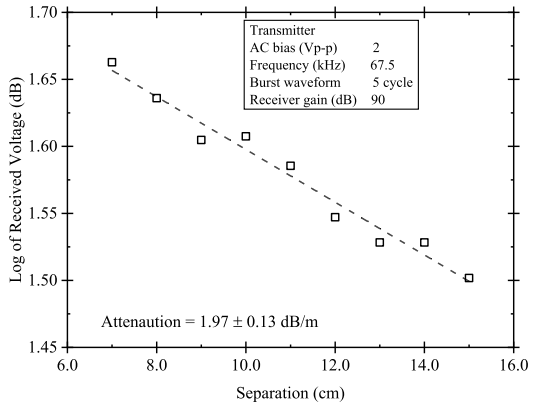

FIGURE 14. Attenuation measurement.

As seen from the Figs. 12-14, the measured sound velocity is 342.5 m/sec and attenuation rate is 1.97 dB/m from a 170 μm radius devices, much smaller than devices mentioned in [13], [17], and [18]. The measured values agree well with published velocity values of 343 m/sec and attenuation factor of 2.38 dB/m [24], based on the laboratory conditions, see ISO 9613-1. These are found for an estimated atmospheric pressure of ∼100 kPa, at the 67.5 kHz supply frequency. Therefore, the CMUT devices proposed in this paper can be effectively used in Martian environment to estimate the wind speed.

V. CONCLUSION

The 2D CMUT based anemometer are designed and developed for Martian environment. The proposed devices are evaluated for their performance in lab environment. The experimental results show that there is a good agreement between the simulated and measured results, presented in this paper. The smaller dimension and lower operating voltages of the devices makes it feasible for their portability and battery operation. The variations in resonant frequency as a function of DC bias are easily observed for the single device and for that connected in an array. These devices, under proper DC bias, operate at frequencies less than 100 kHz, suited for the Martian anemometry. The challenge to fabricate and bias membrane devices of such a diameter and size was resolved by increasing the size of annular membrane anchor. Having smaller device dimension was very important, such that maximum devices can be packed in a 5×5 mm chip area, maintaining a small overall chip area. As such, the 1D array, not described here, had 10 devices and the 2D array was limited to a size of 3×10 devices. Having such device and array dimensions, also allowed for the incorporation of the on-chip test structures and individual devices with varied radii, not presented in this paper. The on-chip test structures facilitated thickness measurement of various layers of the fabricated PolyMUMPs chip.

As shown in Figs. 4, 7, and 11, it is possible to build low frequency CMUTs, that are small enough as compared to research done in [13], [17], and [18], yet can sustain supply and acoustic vibrations. The devices showed good acoustic characteristics, comparable with the standard values, which can further aid Martian anemometry experiments.

ACKNOWLEDGMENT

The authors would like to thank Daryl Hamelin for his support and contribution to setup the test and measurement system. The authors would also like to thank CMC Microsystems for their support related to COMSOL licensing and PolyMUMPs chip fabrication and packaging. VN Instruments are also acknowledged for providing them with their equipment.

REFERENCES

[1] D. Banfield, D. W. Schindel, S. Tarr, and R. W. Dissly, "A Martian acoustic anemometer," *J. Acoust. Soc. Amer.*, vol. 140, no. 2, pp. 1420–1428, Aug. 2016.
[2] W. B. Hess, R. C. Swengel, and S. K. Waldorf, "Measuring water velocity by ultrasonic method," *Electr. Eng.*, vol. 69, no. 11, p. 983, 1950.
[3] E. Hiedemann, "Ultrasonic stroboscope," in *Proc. IRE Natl. Conv. Rec.*, 1956, pp. 38–44.
[4] Ö. Oralka, "Capacitive micromachined ultrasonic transducers: Next-generation arrays for acoustic imaging?" *IEEE Trans. Ultrason., Ferroelectr., Freq. Control*, vol. 49, no. 11, pp. 1596–1610, Nov. 2002.
[5] D. Banfield and R. Dissly, "A Martian sonic anemometer," in *Proc. IEEE Aerosp. Conf.*, Mar. 2005, pp. 641–647.

[6] A. Ghahramani, M. Zhu, R. J. Przybyla, M. P. Andersen, P. J. Galicia, T. E. Peffer, H. Zhang, and E. Arens, "Measuring air speed with a low-power MEMS ultrasonic anemometer via adaptive phase tracking," *IEEE Sensors J.*, vol. 19, no. 18, pp. 8136–8145, Sep. 2019.

[7] T. E. Chamberlain, H. L. Cole, R. G. Dutton, G. C. Greene, and J. E. Tillman, "Atmospheric measurements on Mars: The Viking meteorology experiment," *Bull. Amer. Meteorol. Soc.*, vol. 57, no. 9, pp. 1094–1104, Sep. 1976.

[8] *Piezoelectric Ceramic Transducers*. Accessed: Feb. 19, 2019. [Online]. Available: http://www.gsc-tech.com/Data_sheet/Piezo/Piezeo-catalog.pdf

[9] H. Hoshyarmanesh, A. Abbasi, P. Moein, M. Ghodsi, and K. Zareinia, "Design and implementation of an accurate, portable, and time-efficient impedance-based transceiver for structural health monitoring," *IEEE/ASME Trans. Mechatronics*, vol. 22, no. 6, pp. 2809–2814, Dec. 2017.

[10] S. Na, Z. Li, L. L. P. Wong, A. I.-H. Chen, M. Macecek, and J. T. W. Yeow, "An optimization and comparative study of air-coupled CMUT cells with circular and annular geometries," *IEEE Trans. Ultrason., Ferroelectr., Freq. Control*, vol. 64, no. 11, pp. 1723–1734, Nov. 2017.

[11] A. Buhrdorf, L. Tebje, O. Ahrens, O. Glitza, and J. Binder, "Capacitive micromachined ultrasonic transducer (CMUT) array for the frequency range below 500 kHz," in *Proc. IEEE Ultrason. Symp.*, Oct. 2000, pp. 915–918.

[12] T. A. Emadi and D. A. Buchanan, "Design and characterization of a capacitive micromachined transducer with a deflectable bottom electrode," *IEEE Electron Device Lett.*, vol. 36, no. 6, pp. 612–614, Jun. 2015.

[13] Y. Huang, A. S. Ergun, E. Haeggstrom, and B. T. Khuri-Yakub, "Fabrication of capacitive micromachined ultrasonic transducers (CMUTs) using wafer bonding technology for low frequency (10 kHz-150 kHz) sonar applications," in *Proc. MTS/IEEE*, vol. 4, Oct. 2002, pp. 2322–2327.

[14] I. Ladabaum, X. Jin, H. T. Soh, A. Atalar, and B. T. Khuri-Yakub, "Surface micromachined capacitive ultrasonic transducers," *IEEE Trans. Ultrason., Ferroelectr., Freq. Control*, vol. 45, no. 3, pp. 678–690, May 1998.

[15] M. S. Salim, M. F. A. Malek, R. B. W. Heng, K. M. Juni, and N. Sabri, "Capacitive micromachined ultrasonic transducers: Technology and application," *J. Med. Ultrasound*, vol. 20, no. 1, pp. 8–31, Mar. 2012.

[16] A. S. Ergun, G. G. Yaralioglu, O. Oralkan, and B. T. Khuri-Yakub, "Techniques and applications of capacitive micromachined ultrasonic transducers," in *MEMS/NEMS Techniques and Application*, vol. 2, C. T. Leondes, Ed. New York, NY, USA: Springer, 2006, pp. 223–285.

[17] I. O. Wygant, M. Kupnik, J. C. Windsor, W. M. Wright, and M. S. Wochner, "50 kHz capacitive micromachined ultrasonic transducers for generation of highly directional sound with parametric arrays," *IEEE Trans. Ultrason., Ferroelectr., Freq. Control*, vol. 56, no. 1, pp. 193–203, Jan. 2009.

[18] S. Na, A. I.-H. Chen, L. L. P. Wong, Z. Li, M. Macecek, and J. T. W. Yeow, "Capacitive micromachined ultrasonic transducers based on annular cell geometry for air-coupled applications," *Ultrasonics*, vol. 71, pp. 152–160, Sep. 2016.

[19] L. T. Elkins-Tanton, *The Solar System MARS*. London, U.K.: Chelsea House, 2006.

[20] J. Carter, A. Cowen, B. Hardy, R. Mahadevan, M. Stonefield, and S. Wilcenski, *PolyMUMPs Design Handbook*, 11th ed. Triangle Park, NC, USA: MEMSCAP, 2013.

[21] M. B. Thacker and D. A. Buchanan, "Design and characterization of low frequency capacitive micromachined ultrasonic transducer (CMUT)," in *Proc. IEEE Int. Conf. Syst., Man, Cybern. (SMC)*, Oct. 2020, vol. 2, no. 1, pp. 2876–2881.

[22] A. Logan and J. T. Yeow, "Fabricating capacitive micromachined ultrasonic transducers with a novel silicon-nitride-based wafer bonding process," *IEEE Trans. Ultrason., Ferroelectr., Freq. Control*, vol. 56, no. 5, pp. 1074–1084, May 2009.

[23] C. J. Hellier, *Handbook of Nondestructive Evaluation*. New York, NY, USA: McGraw-Hill, 2001.

[24] *ISO 9613 Part 1*. Accessed: Sep. 19, 2020. [Online]. Available: http://resource.npl.co.uk/acoustics/techguides/absorption/

MAYANK B. THACKER (Graduate Student Member, IEEE) received the B.E. and M.Tech. degrees form RTM Nagpur University, Nagpur, Maharashtra, India, in 2009 and 2013, respectively. He is currently a Graduate Student with the University of Manitoba, Winnipeg, Canada.

He worked as an Assistant Professor with the Electronics Engineering Department, Shri Ramdeobaba College of Engineering and Management, Nagpur, for over five years (2009–2011 and 2013–2016). His research interests include MOS-based low noise amplifier, operational transconductance amplifier, and MEMS.

Mr. Thacker is a Life Member of the Indian Society for Technical Education (ISTE) and the Institute of Smart Structures and Systems (ISSS).

AREZOO EMADI (Senior Member, IEEE) received the Ph.D. degree from the Department of Electrical and Computer Engineering, University of Manitoba, and the Licentiate degree from the Department of Microtechnology and Nanoscience, Chalmers University of Technology.

She is currently an Associate Professor with the Department of Electrical and Computer Engineering. Her research interests include the area of micro electromechanical systems (MEMS), medical MEMS sensors and transducers, bio and chemical sensors, advanced diagnosis sensor technologies, micro and nano electronic devices, and fabrication and medical imaging systems.

Dr. Emadi is a Professional Engineer (P.Eng.).

DOUGLAS A. BUCHANAN (Senior Member, IEEE) received the B.Sc. and M.Sc. degrees from the University of Manitoba, Winnipeg, MB, Canada, in 1981 and 1982, respectively, and the Ph.D. degree from the University of Durham, Durham, U.K., in 1986.

Following his Ph.D. studies on electronic conduction in silicon-rich thin films, he spent 16 years (1986–2002) at IBM Thomas J. Watson Research Center. He worked on reliability and degradation of many MOSFET generations. He also worked on the development of first high-k gate insulator in an 80 nm FET and on quantum mechanical tunneling in ultrathin gate dielectrics. He is currently a Professor with the Electrical and Computer Engineering Department, University of Manitoba. He holds over 32 patents, over 110 peer-reviewed publications, and over 100 conference presentations.

Dr. Buchanan is a fellow of the Canadian Academy of Engineering and a Professional Engineer (P.Eng.).